AGU PUBLICATIONS

Geophysical Research Letters

RESEARCH LETTER
10.1002/2016GL070114

Key Points:
- First long-term time series of NH_3 concentrations in the high Arctic
- Boreal wildfire emissions of NH_3 detected in Canadian Arctic and Southern Canada
- 2014 Northwest Territories fires were a considerable source of NH_3 in the summertime Arctic

Supporting Information:
- Supporting Information S1

Correspondence to:
E. Lutsch,
elutsch@physics.utoronto.ca

Citation:
Lutsch, E., E. Dammers, S. Conway, and K. Strong (2016), Long-range transport of NH_3, CO, HCN, and C_2H_6 from the 2014 Canadian Wildfires, *Geophys. Res. Lett.*, *43*, 8286–8297 doi:10.1002/2016GL070114.

Received 24 JUN 2016
Accepted 19 JUL 2016
Accepted article online 23 JUL 2016
Published online 4 AUG 2016

Long-range transport of NH_3, CO, HCN, and C_2H_6 from the 2014 Canadian Wildfires

E. Lutsch[1], E. Dammers[2], S. Conway[1], and K. Strong[1]

[1]Department of Physics, University of Toronto, Toronto, Ontario, Canada, [2]Cluster Earth and Climate, Department of Earth Sciences, Vrije Universiteit Amsterdam, Amsterdam, Netherlands

Abstract We report the first long-term measurements of ammonia (NH_3) in the high Arctic. Enhancements of the total columns of NH_3, carbon monoxide (CO), hydrogen cyanide (HCN), and ethane (C_2H_6) were detected in July and August 2014 at Eureka, Nunavut, and Toronto, Ontario. Enhancements were attributed to fires in the Northwest Territories using the FLEXPART Lagrangian dispersion model and the Moderate Resolution Imaging Spectroradiometer Fire Hot Spot data set. Emission estimates are reported as average emission factors for HCN (0.62 ± 0.34 g kg^{-1}), C_2H_6 (1.50 ± 0.75 g kg^{-1}), and NH_3 (1.40 ± 0.72 g kg^{-1}). Observations of NH_3 at both sites demonstrate long-range transport of NH_3, with an estimated NH_3 lifetime of 48 h. We also conclude that boreal fires may be an important source of NH_3 in the summertime Arctic.

1. Introduction

The Arctic has few sources of ammonia (NH_3), with the main sources being seabird guano [*Blackall et al.*, 2007] and seal excreta [*Theobald et al.*, 2006]. Although biomass burning has been identified as a significant source of NH_3 [*Bouwman et al.*, 1997], its short lifetime, typically under 24 h, would make long-range transport from lower latitudes to the Arctic unlikely [*Lefer et al.*, 1999]. Emissions of NH_3 from boreal fires in Canada and Alaska have been previously measured by aircraft-based in situ instruments [*Nance et al.*, 1993] and airborne Fourier transform infrared (FTIR) spectroscopy [*Goode et al.*, 2000]. Satellite observations have also quantified boreal fire emissions of NH_3, including Tropospheric Emission Spectrometer (TES) measurements of NH_3 from Alaskan fires [*Alvarado et al.*, 2011] and Infrared Atmospheric Sounding Interferometer (IASI) measurements from the 2010 Russian fires [*R'Honi et al.*, 2013]. These studies have attempted to quantify NH_3 emissions from boreal fires; however, possible long-range transport of NH_3 to the Arctic has not yet been investigated.

Atmospheric NH_3 reacts rapidly with acidic gases in the atmosphere leading to the formation of particulate matter [*Behera et al.*, 2013; *Hertel et al.*, 2012] which contribute to a reduction in air quality [*Pope et al.*, 2009; *Erisman et al.*, 2011]. NH_3 is also known to contribute to the acidification and eutrophication of soil and water bodies therefore affecting biodiversity [*Bobbink et al.*, 1998, 2010], while in high concentrations NH_3 is toxic to living organisms. Transport of NH_3 to the Arctic will thus affect air quality, while deposition of NH_3 could influence biodiversity in this sensitive ecosystem. However, the effects of NH_3 in the Arctic remain unknown as its abundance, sources, and sinks have not yet been quantified in this region.

Measurement of NH_3 is difficult due to its low ambient concentrations and episodic emissions. Although satellite observations, such as those from TES and IASI, provide global coverage, NH_3 measurements are limited in high-latitude regions due to insufficient thermal contrast and low concentrations, even during fire-enhanced periods. The first measurements of NH_3 in the Canadian Arctic were performed by *Wentworth et al.* [2016], who made shipborne measurements of boundary layer NH_3 from 13 July to 7 August 2014. During this period, boreal fires were burning in the Northwest Territories, although the main source of NH_3 was attributed to seabirds. It is likely that shipborne measurements have limited sensitivity to biomass burning emissions as these would be more abundant in the free troposphere than in the boundary layer. For this reason, total column measurements of NH_3 are preferable for quantifying fire emissions of NH_3.

It has been recently shown that solar absorption spectroscopy using FTIR spectrometers can be used to measure NH_3 total columns [*Dammers et al.*, 2015], while biomass burning emissions of carbon monoxide (CO), hydrogen cyanide (HCN) and ethane (C_2H_6) have been previously measured in the Canadian Arctic at Eureka [*Viatte et al.*, 2013, 2014, 2015], Australia [*Paton-Walsh et al.*, 2005, 2010], Reunion Island [*Vigouroux et al.*, 2012],

and Japan [*Zhao et al.*, 2002]. The ground-based FTIR instrument at Eureka provides measurements of NH_3 where satellite observations and in situ data are sparse or nonexistent.

In this paper, two FTIR instruments at Eureka, Nunavut, and Toronto, Ontario, were used to detect NH_3 emissions from the 2014 Northwest Territories fires. The fire source near Great Slave Lake (61.67°N, 114.00°W) is approximately 2300 km and 3100 km from Eureka and Toronto, respectively. NH_3 was measured at both sites, with detection of total column enhancements 2–5 times the background during the burning period. Simultaneous enhancements of CO, HCN, and C_2H_6 on the order of 1.5–2 times the background were also observed, providing further indication of long-range transport of fire emissions. The spatial separation between sites and differences in travel times of the smoke plume also allowed for an NH_3 lifetime of 48 h to be estimated. The enhancements at Eureka confirm the possibility of long-range transport of NH_3 and suggest that boreal fires may be a significant episodic source of NH_3 in the summertime Arctic.

2. Methods

2.1. Sites and Instruments

Trace gas column amounts are retrieved from solar absorption spectra obtained by two FTIR spectrometers: a Bruker IFS 125HR at the Polar Environment Atmospheric Research Laboratory (PEARL) in Eureka, Nunavut (80.05°N, 86.42°W) and an ABB Bomem DA8 at the University of Toronto Atmospheric Observatory (TAO) in Toronto, Ontario (43.66°N, 79.40°W). Measurements from both instruments are contributed to the Network for Detection of Atmospheric Composition Change (NDACC; http://www.ndsc.ncep.noaa.gov/). A detailed instrument description of the Bruker 125HR at PEARL is given by *Batchelor et al.* [2009]. Measurements are made in the midinfrared at a resolution of 0.0035 cm^{-1} using a KBr beam splitter and either an InSb or HgCdTe detector and a series of optical filters. A detailed description of the Bomem DA8 at TAO is given by *Wiacek et al.* [2007] and *Whaley et al.* [2015]. Measurements are made with the same optical components and resolution as the PEARL instrument. For both instruments, spectra are recorded continuously during clear-sky daylight hours by alternating between optical filters while a heliostat system tracks the Sun.

2.2. Retrieval Methods

Solar absorption spectra were processed using the SFIT4 retrieval algorithm (https://wiki.ucar.edu/display/sfit4/). SFIT4 is based on the Optimal Estimation Method [*Rodgers*, 2000] which iteratively adjusts trace gas volume mixing ratio profiles to minimize the difference between the measured and calculated spectra [*Pougatchev et al.*, 1995; *Rinsland et al.*, 1998]. The forward model of SFIT4 is a line-by-line radiative transfer model that uses a Voigt line shape. Temperature and pressure profiles are provided by the National Centers for Environmental Prediction (NCEP) and spectroscopic parameters from HITRAN 2008 [*Rothman et al.*, 2009] are used.

CO, HCN, and C_2H_6 are standard NDACC Infrared Working Group (IRWG, https://www2.acom.ucar.edu/irwg) products. These species were retrieved using IRWG-recommended microwindows and a priori profiles. For each site, 40 year average (1980–2020) profiles from the Whole-Atmosphere Community Climate Model (WACCM V6) [*Eyring et al.*, 2007] were used as the a priori profiles for these species. Three microwindows were used for CO: a strong line at 2157.51–2159.14 cm^{-1} and two weak lines at 2057.68–2058.00 and 2069.56–2069.76 cm^{-1} [*Notholt et al.*, 2000; *Zhao et al.*, 2002]. For HCN, three microwindows were used: 3268.00–3268.38, 3287.00–3287.48, and 3299.40–3299.60 cm^{-1} [*Notholt et al.*, 2000; *Zhao et al.*, 2002; *Mahieu et al.*, 1997]. Three microwindows were also used for C_2H_6: 2976.66–2976.95 [*Mahieu et al.*, 1997; *Rinsland et al.*, 2002; *Paton-Walsh et al.*, 2010], 2983.20–2983.55 [*Meier et al.*, 2004], and 2986.50–2986.95 cm^{-1} [*Notholt et al.*, 1997].

The microwindows used for NH_3 correspond to the absorption lines of the ν_2 vibrational band [*Dammers et al.*, 2015]. For Eureka, three microwindows were used: 929.40–931.40, 950.02–952.20, and 962.10–970.00 cm^{-1}. The first and last microwindows for Eureka were also used for Toronto but narrowed to 930.32–931.32 and 966.97–967.68 cm^{-1}, respectively, due to water vapor interference. The 950.02–952.20 cm^{-1} microwindow was not used for Toronto as a result of saturation due to water vapor. The use of three microwindows at Eureka was necessary in order to achieve adequate information content due to the low NH_3 concentrations. For both sites, the NH_3 a priori profile was derived from balloon-based measurements [*Toon et al.*, 1999] taken near Fairbanks, Alaska (64.84°N, 147.72°W).

For all retrievals, full error analysis was performed following *Rodgers* [2000]. The retrieval uncertainties include smoothing error due to the limited vertical resolution, forward model parameter error, and measurement

noise error. Adding these in quadrature, average uncertainties for the retrieved total columns of CO, HCN, C_2H_6, and NH_3 are 3.4%, 10.3%, 1.1%, and 26.7%, respectively, for Eureka and 3.2%, 6.4%, 5.4%, and 20.2%, respectively, for Toronto. The average degrees of freedom for signal for CO, HCN, C_2H_6, and NH_3 are 2.4, 1.8, 1.3, and 1.1, respectively, for Eureka and 3.5, 2.2, 1.9, and 1.1, respectively, for Toronto. For CO, HCN, and C_2H_6, the total column averaging kernels (shown in the supporting information) show peak values in the upper troposphere at both sites, while the total column averaging kernels of NH_3 peak near the surface and decrease upward to 5 km. Differences in the total column averaging kernels between species were not taken into account in the analysis below, as CO, HCN, and C_2H_6 have similar vertical sensitivities. However, for NH_3, the contribution to its total column from altitudes above 5 km could be underestimated as a result of the lack of vertical sensitivity in this region.

3. Results and Discussion

3.1. FTIR Time Series

The total column time series for CO, HCN, C_2H_6, and NH_3 at Eureka and Toronto are shown in Figure 1. All years (2006–2014 for Eureka and 2002–2014 for Toronto) are shown in gray, while 2014 measurements are highlighted in red for Eureka and blue for Toronto. The maximum monthly mean CO total columns are observed in March at Eureka (2.07×10^{18} molecules cm^{-2}) and April at Toronto (2.41×10^{18} molecules cm^{-2}). Minimum monthly mean total columns are observed in September at Eureka (1.59×10^{18} molecules cm^{-2}) and Toronto (1.85×10^{18} molecules cm^{-2}). The main sources of CO are fossil fuel combustion and oxidation of volatile organic compounds and CH_4, as well as biomass burning emissions [*Holloway et al.*, 2000]. The primary sink of CO is oxidation by hydroxyl (OH) which contributes to the seasonal cycle at both sites. Larger total columns of CO are observed for Toronto due to nearby anthropogenic sources. Transport of CO from midlatitudes also contributes to the seasonal cycle at Eureka, while biomass burning emissions are observed in the summer months.

Maximum monthly mean total columns of HCN are observed in August at Eureka (6.8×10^{15} molecules cm^{-2}) and July at Toronto (6.79×10^{15} molecules cm^{-2}). Since HCN is relatively inactive, it serves as a good tracer of biomass burning [*Rinsland et al.*, 2001]. Additional sources are the result of emissions from plants, bacteria, and fungi due to increased vegetative activity in the springtime [*Cicerone and Zellner*, 1983]. The lifetime of HCN in the troposphere is approximately 5 months [*Li et al.*, 2003], with main sinks due to OH and $O(^1D)$ reaction [*Cicerone and Zellner*, 1983] and ocean uptake [*Li et al.*, 2003]. Large variability of HCN is observed in the summer months at Eureka corresponding to the boreal fire season from May to August [*Macias Fauria and Johnson*, 2008]. Particularly, large fire events in Russia during July 2008 and August 2010 are observed in the time series [*Viatte et al.*, 2013, 2015] in addition to the 2014 Northwest Territories fires.

The sources of C_2H_6 are natural gas and fossil fuel emissions [*Singh and Zimmerman*, 1992] in addition to biomass burning, while its main sink is reaction with OH. The seasonal cycle of C_2H_6 is similar to that of CO due to their common sources and sinks. Maximum monthly mean total columns are observed in March at Eureka (2.67×10^{16} molecules cm^{-2}) and February at Toronto (2.97×10^{16} molecules cm^{-2}) with minima in August at Eureka (1.2×10^{16} molecules cm^{-2}) and Toronto (1.49×10^{16} molecules cm^{-2}). Both CO and C_2H_6 have relatively long atmospheric lifetimes at 52 days [*Daniel and Solomon*, 1998] and 80 days [*Xiao et al.*, 2008], respectively.

The time series of NH_3 at Eureka and Toronto show maximum monthly mean total columns in the summer months (2.79×10^{14} molecules cm^{-2} in July at Eureka and 9.80×10^{15} molecules cm^{-2} in May at Toronto) as a result of its biogenic sources, biomass burning, and agricultural emissions. The lower abundance of NH_3 at Eureka is due to its isolation from nearby sources. However, it has been suggested that seabird colonies may be a considerable source of NH_3 in the Arctic [*Wentworth et al.*, 2016]. For both sites, NH_3 is highly variable due to its short lifetime and its emissions being rather episodic in nature. For both Eureka and Toronto, large enhancements of NH_3 are observed in July and August 2014 due to boreal fires in the Northwest Territories as shown in section 3.2.

3.2. Source Attribution

Enhancements in the time series of each species were first identified by measurements with a total column greater than a 3σ deviation from the monthly mean taken over all years. By this criterion, three main enhancements were found for each site in July and August 2014. The first initial detection for Eureka occurred on 25 July 2014 (14:40 UTC) which corresponds to the maximum CO total column measured on that day. Two later enhancements were also detected at Eureka on 7 August 2014 (17:20 UTC) and 19 August 2014 (19:15 UTC).

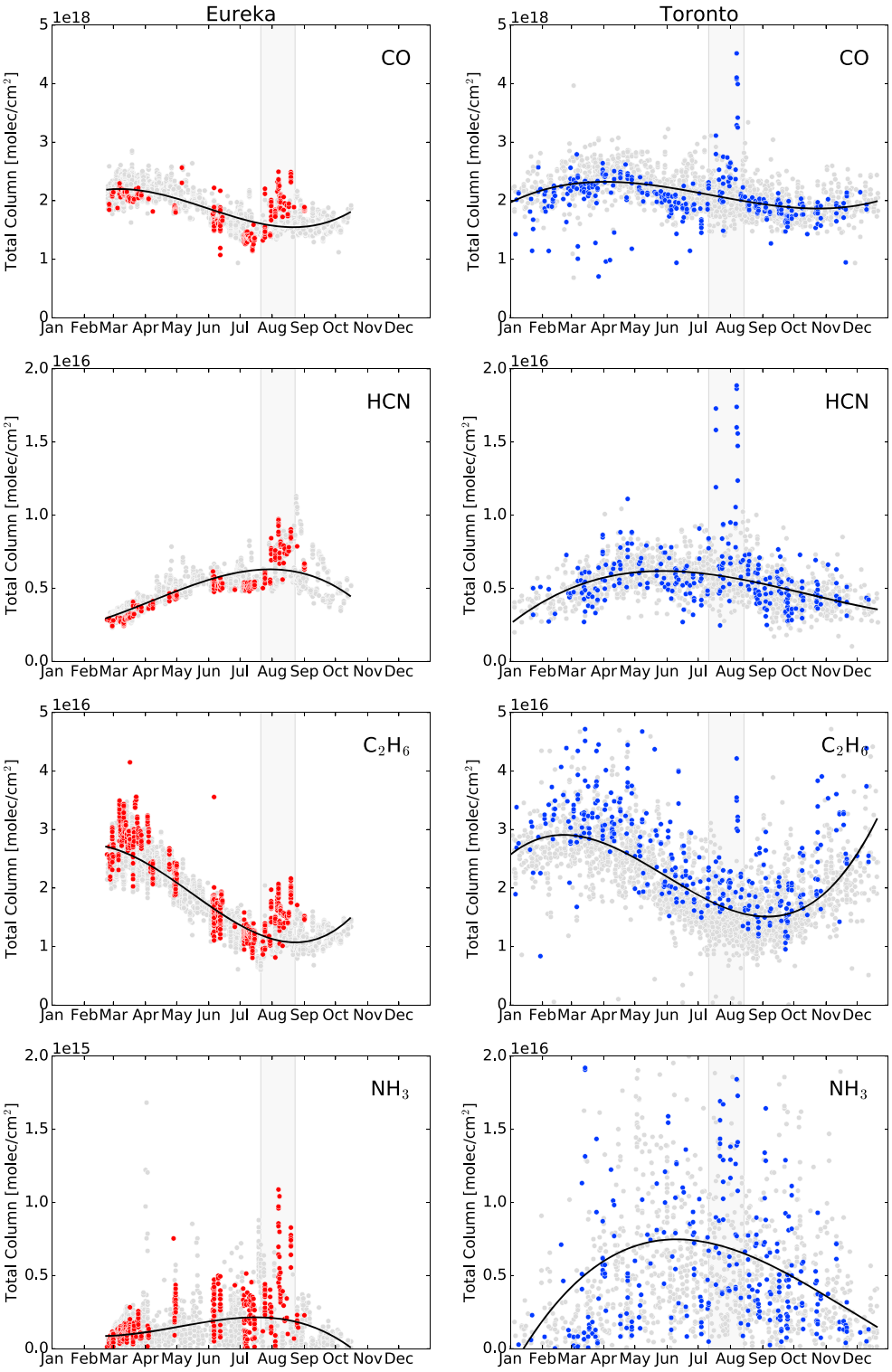

Figure 1. Total column time series of CO, HCN, C_2H_6, and NH_3 for (left) Eureka (2006–2014) and (right) Toronto (2002–2014). All years are shown in gray, while 2014 is highlighted. The gray vertical bar indicates periods of fire-affected measurements (25 July to 22 August for Eureka and 11 July to 13 August for Toronto). The black line represents a polynomial fit to the data for all years.

Similarly, the initial enhancement at Toronto was found to have occurred on 11 July 2014 (14:09 UTC) with two later maxima on 18 July 2014 (19:05 UTC) and 7 August 2014 (17:20 UTC).

To determine the source of the observed enhancements, the FLEXPART [*Stohl et al.*, 2005] Lagrangian dispersion model was used. Backward dispersion runs were initialized by releasing an ensemble of 60,000 air-tracer particles over a 6 h period about the observed peak enhancement for CO. The particles were released over a 3° × 3° box centered on each site. The model was run backward in time for 7 days driven by meteorological data from the NCEP Climate Forecast System (CFS V2) 6 h product [*Saha et al.*, 2011]. The FLEXPART model was run for each of the three peak enhancements observed at both sites.

The sensitivity of the measurement to various source regions is proportional to the residence time of the air-tracer particles. The FLEXPART sensitivities are shown in Figure 2 for both sites. The Moderate Resolution Imaging Spectroradiometer (MODIS) Active Fire data [*Giglio et al.*, 2006] provide the locations of active fires as shown in Figure 2. The FIRMS (Fire Resource Management System, https://earthdata.nasa.gov/earth-observation-data/near-real-time/firms/active-fire-data) fire product was used, where the plotted points correspond to fire detections with a confidence ratio of 0.75 or greater. For all FLEXPART backward runs, sensitivity to the Northwest Territories fires is observed. The initial enhancements on 25 July 2014 for Eureka and 11 July 2014 for Toronto show the least sensitivity to these fires, while the greatest sensitivity is observed in the 7 August 2014 FLEXPART runs for both sites, which is consistent with the largest enhancements observed at that time.

3.3. Trace Gas Correlations

The enhancement ratio (EnhR) is used to quantify emissions from biomass burning events for periods of fire-affected measurements. Fire-affected measurements were first classified as those with total column amounts greater than a 1σ standard deviation from the monthly mean over all years. Since each species was retrieved in a different spectral region measured using optical filters, the enhancement ratio was limited to measurements occurring within 1 h of a CO measurement, where each CO measurement was only used once in the correlation. The correlations of HCN, C_2H_6, and NH_3 with CO for Eureka and Toronto are shown in Figure 3. The colored points represent fire-affected measurements from 25 July to 22 August 2014 for Eureka (red) and 11 July to 13 August 2014 for Toronto (blue). For C_2H_6, there is a linear trend for all measurements as a result of the similar seasonal cycles of CO and C_2H_6. No trend is observed for HCN and NH_3 with CO due to their differing seasonal cycles.

The unified least squares procedure of *York et al.* [2004], which accounts for errors in both the ordinal and abscissa coordinates, was used to determine a linear regression for the fire-affected measurements. The result of the linear regression is shown as the dashed line in Figure 3, the slope of which is the enhancement ratio of the target species. The uncertainty of the enhancement ratio is the standard error of the slope given by *York et al.* [2004]. There is generally a good correlation with CO for HCN and C_2H_6 with correlation coefficients ranging from 0.70 to 0.93. For NH_3, the correlation coefficient is 0.70 for Eureka and 0.45 for Toronto. The lower correlation for Toronto NH_3 measurements is likely due to the variability of the total column amounts of NH_3 due to nearby agricultural and anthropogenic sources.

Since measurements are made at a distance from the fire source, the measured smoke plumes have experienced aging, resulting in some loss of each species. Aging of the plume is accounted for by calculation of the emission ratio (ER) at the fire source assuming a first-order loss of each species. The emission ratio is defined by

$$\mathrm{ER}_X = \mathrm{EnhR}_X \cdot \frac{\exp\left(\frac{t}{\tau_X}\right)}{\exp\left(\frac{t}{\tau_{\mathrm{CO}}}\right)}, \tag{1}$$

where τ_X is the lifetime of the species and t is the travel time. Lifetimes for CO, HCN, and C_2H_6 were chosen to be 30, 75, and 45 days, respectively, following *Viatte et al.* [2015], which were determined by model comparisons to FTIR measurements. The travel times to each site were determined by HYbrid Single-Particle Lagrangian Integrated Trajectory (HYSPLIT) [*Rolph*, 2016; *Stein et al.*, 2015] back trajectories. For each of the three peak CO enhancements at each site described in section 3.2, the HYSPLIT model was run backward in time for 10 days. For each HYSPLIT model run, three trajectory altitudes between 3 and 10 km were used. The start time of each model run was adjusted to within 2 h of the observed peak CO enhancement, while the trajectory altitudes were also adjusted in order to provide back trajectories that were consistent with the fire source

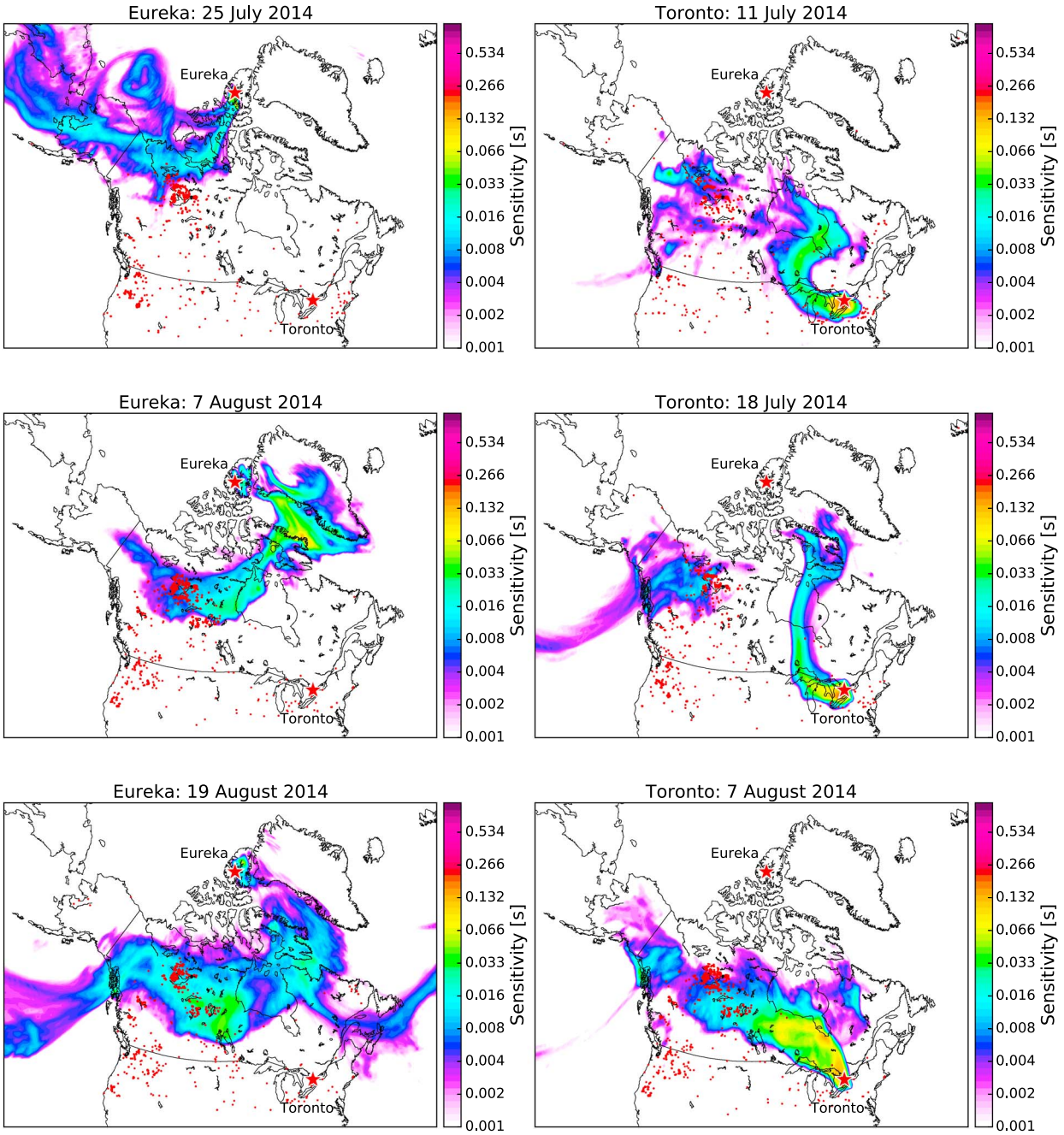

Figure 2. FLEXPART backward dispersion runs showing the total column sensitivity. MODIS fire hot spots are shown in red for 7 days prior to the release time. Particle release times for each panel correspond to the main CO enhancements observed at each site. Each panel represents a single FLEXPART model run, run backward in time for 7 days starting at the initial particle release.

regions identified by the FLEXPART model runs and MODIS fire data. From the three HYSPLIT model runs for each site, an average travel time was found to be 6 days for Eureka and 3 days for Toronto, with a standard deviation of 2 days and 1 day for Eureka and Toronto, respectively. The average travel times and standard deviation were determined from the three HYSPLIT runs over three trajectory altitudes. The emission ratios were calculated using these travel times and are shown in Table 1.

Because the travel time is dependent on the meteorological conditions along the trajectory of the smoke plume, it is difficult to account for variations in the travel time during the period of fire-affected measurements. For the long-lived species CO, HCN, and C_2H_6, the variability of the travel times is small compared to

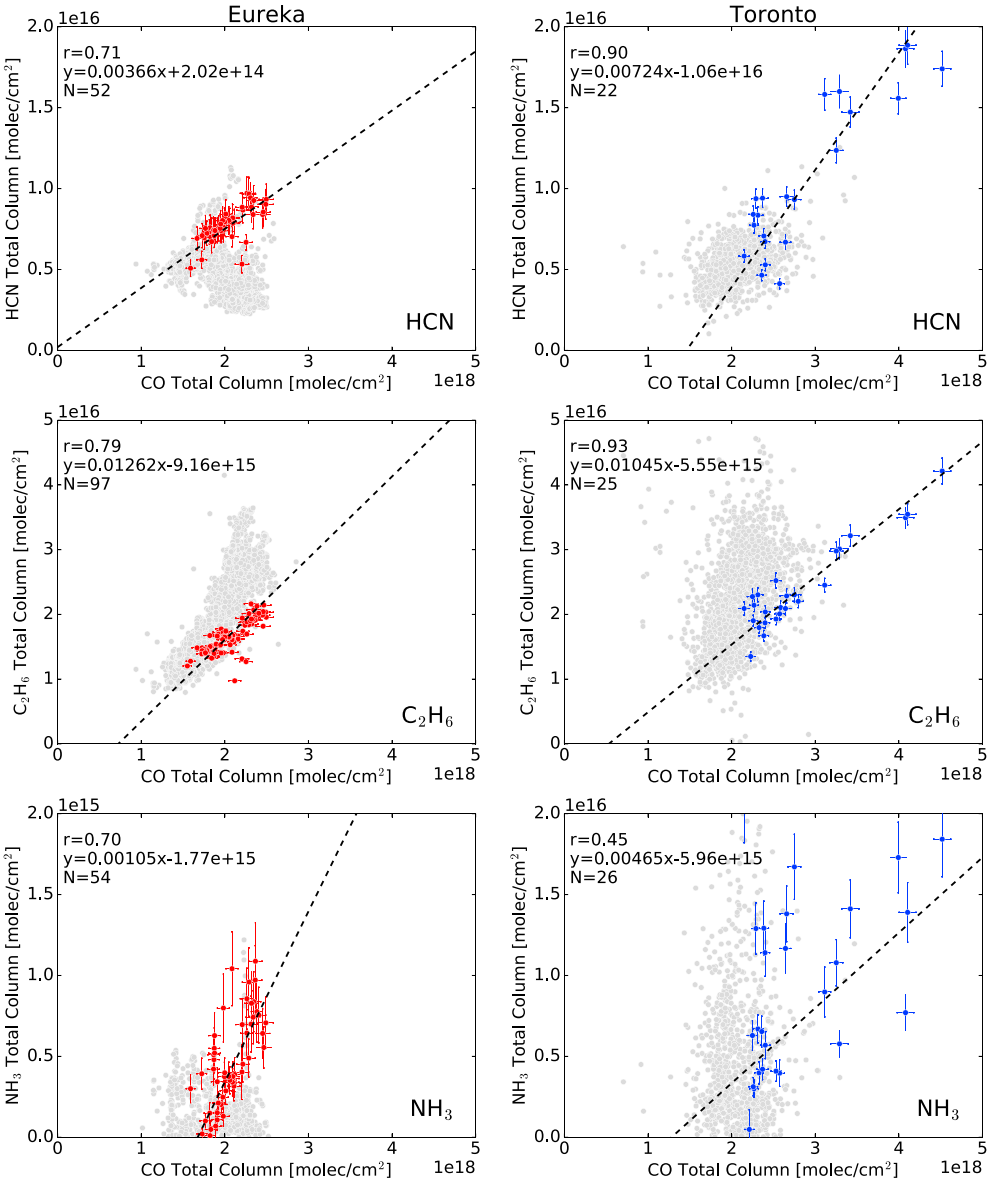

Figure 3. Enhancement ratios for HCN, C_2H_6, and NH_3 for fire-affected measurements (25 July to 22 August 2014 for Eureka in red and 11 July to 13 August for Toronto in blue). The gray points represent all other measurements. The correlation coefficient *r*, linear equation of the fit, and number of fire-affected measurements are shown. Error bars correspond to the retrieval uncertainties for the respective species.

the lifetime of each species. It was found that the variability in the emission ratios for HCN and C_2H_6 due to the estimated variability of the travel times was within the uncertainties due to the enhancement ratios. For NH_3, the assumed lifetimes vary from 12 to 48 h and are comparable to the estimated travel times. Assuming this range of NH_3 lifetimes, the emission ratios were found to vary over several orders of magnitude for a single travel time. The variability of the emission ratio due to the estimated variability of the travel times for a single NH_3 lifetime was within this range. It was therefore concluded that the lifetime of NH_3 was the dominant source of uncertainty on the emission ratio. For these reasons, we have chosen the enhancement ratio uncertainty as the predominant uncertainty in the calculation of the emission ratio for all species.

For HCN, the emission ratios differ between Eureka (0.0037 $\pm$ 0.0005) and Toronto (0.0072 $\pm$ 0.0003) with a relative difference of approximately 82%, while a relative difference of 7% is found for the emission ratios of C_2H_6 at Eureka (0.0109$\pm$0.0004) and Toronto (0.0101$\pm$0.0005). The large difference in the HCN emission ratios suggests that additional sources of HCN were present for Toronto. This is evident in the FLEXPART sensitivities

Table 1. Comparison of Calculated Enhancement Ratios, Emission Ratios, and Emission Factors for HCN, C_2H_6, and NH_3 at Eureka and Toronto[a]

			Eureka			Toronto		
Source	Platform	EF_{CO} (g kg^{-1})	EnhR	ER	EF (g kg^{-1})	EnhR	ER	EF (g kg^{-1})
				HCN				
This study	Ground-based	127 (45)[b]	0.0037 (0.0005)	0.0032 (0.0005)	0.40 (0.15)	0.0072 (0.0003)	0.0068 (0.0003)	0.84 (0.30)
Akagi et al. [2011]	Compilation	127 (45)	–	–	1.52 (0.81)	–	–	1.52 (0.81)
Andreae and Merlet [2001][c]	Compilation	107 (37)	–	–	0.81	–	–	0.81
Viatte et al. [2015][d]	Ground-based	127 (45)	–	0.0034 (0.0009)	0.36 (0.17)	–	0.0034 (0.0009)	0.36 (0.17)
Goode et al. [2000][e]	Aircraft	88.8	–	0.0069	0.61	–	0.0069	61
Simpson et al. [2011][f]	Aircraft	112 (72)	–	0.0082 (0.0002)	0.89 (0.29)	–	0.0082 (0.0002)	0.89 (0.29)
Rinsland et al. [2007][g]	Satellite	86 (17)	–	0.0024 (0.0003)	0.20 (0.05)	–	0.0024 (0.0003)	0.20 (0.05)
Tereszchuk et al. [2013][g]	Satellite	–	–	0.0027 (0.0018)	–	–	0.0027 (0.0018)	–
				C_2H_6				
This study	Ground-based	127 (45)[b]	0.0126 (0.0005)	0.0118 (0.0005)	1.61 (0.57)	0.0104 (0.0005)	0.0101 (0.0005)	1.38 (0.49)
Akagi et al. [2011]	Compilation	127 (45)	–	–	1.42 (0.43)	–	–	1.42 (0.43)
Andreae and Merlet [2001][c]	Compilation	107 (37)	–	–	0.60 (0.15)	–	–	0.60 (0.15)
Viatte et al. [2015][d]	Ground-based	127 (45)	–	0.0096 (0.0031)	1.09 (0.74)	–	0.0096 (0.0031)	1.09 (0.74)
Nance et al. [1993][e]	Aircraft	81 (12)	–	0.0073 (0.0031)	0.66 (0.35)	–	0.0073 (0.0031)	0.66 (0.35)
Goode et al. [2000][e]	Aircraft	88.8	–	0.0073	0.66	–	0.0073	0.66
Simpson et al. [2011][f]	Aircraft	112 (72)	–	0.0046 (0.0009)	0.56 (0.13)	–	0.0046 (0.0009)	0.56 (0.13)
Rinsland et al. [2007][g]	Satellite	86 (17)	–	0.0098 (0.0008)	0.91 (0.19)	–	0.0098 (0.0008)	0.91 (0.19)
Tereszchuk et al. [2013][g]	Satellite	–	–	0.0069 (0.0023)	–	–	0.0069 (0.0023)	–
				NH_3				
This study ($\tau = 36$ h)	Ground-based	127 (45)[b]	0.0011 (0.0001)	0.0471 (0.0039)	3.64 (1.32)	0.0047 (0.0004)	0.0311 (0.0029)	2.40 (0.88)
This study ($\tau = 48$ h)	Ground-based	127 (45)[b]	0.0011 (0.0001)	0.0173 (0.0014)	1.34 (0.49)	0.0047 (0.0004)	0.0189 (0.0018)	1.46 (0.53)
Akagi et al. [2011]	Compilation	127 (45)	–	–	2.72 (2.32)	–	–	2.72 (2.32)
Andreae and Merlet [2001][c]	Compilation	107 (37)	–	–	1.40 (0.80)	–	–	1.40 (0.80)
Nance et al. [1993][e]	Aircraft	81 (12)	–	0.0130 (0.0050)	0.64 (0.31)	–	0.0130 (0.0050)	0.64 (0.31)
Goode et al. [2000][e]	Aircraft	88.8	–	0.0158	0.86	–	0.0158	0.86
Alvarado et al. [2011][h]	Satellite	–	–	0.0100 (0.0050)	–	–	0.0100 (0.0050)	–
R'Honi et al. [2013][i]	Satellite	–	–	0.0310	–	–	0.0310	–

[a]The values in parentheses denote the reported uncertainties.
[b]EF_{CO} for boreal forests from *Akagi et al.* [2011] used for conversion of ER to EF.
[c]Values reported for extratropical forests.
[d]Ground-based FTIR measurements at Eureka, Nunavut.
[e]Measurements from Alaskan fires.
[f]Measurements from Canadian fires.
[g]ACE-FTS observations from Canadian and Alaskan fires.
[h]TES observations from Canadian and Alaskan fires.
[i]Average value from IASI observations of the 2010 Russian fires.

of Figure 2. For each FLEXPART run for Toronto, considerable sensitivity to Northern Ontario and the Great Lakes region of Canada and the United States was observed. In addition, the emission ratios of HCN are an order of magnitude lower than those of C_2H_6 and the influence of additional sources is likely amplified.

Since NH_3 is short lived, plume aging has a significant effect on the measured enhancement ratio. To determine the emission ratios, four lifetimes for NH_3 were chosen: 12, 24, 36, and 48 h. The 12, 24, and 36 h lifetimes were chosen following *Whitburn et al.* [2015] from *Dentener and Crutzen* [1994], *Aneja et al.* [2001], and *R'Honi et al.* [2013], respectively. The 12 h and 24 h NH_3 lifetimes yielded large emission ratios (~10–100) and differed by an order of magnitude between sites. For this reason, these lifetimes were omitted from further analysis and it was inferred that the NH_3 lifetime must be considerably longer. Agreement was found assuming a 36 h lifetime with emission ratios of 0.0471 ± 0.0039 and 0.0311 ± 0.0029 for Eureka and Toronto, respectively.

The best agreement was found assuming a 48 h lifetime, which yielded emission ratios of 0.0173 ± 0.0014 and 0.0189 ± 0.0018 for Eureka and Toronto, respectively.

The assumption of a 48 h NH_3 lifetime is supported by comparison of the emission ratios to previously published values. Emission ratios for NH_3 of 0.0130 ± 0.0050 and 0.0158 were reported by *Nance et al.* [1993] and *Goode et al.* [2000], obtained from aircraft-based measurements of emissions from Canadian and Alaskan fires. The NH_3 emission ratio determined from TES observations of Canadian and Alaskan fires was 0.0100 ± 0.0050 [*Alvarado et al.*, 2011]. Using observations of the 2010 Russian fires from IASI, *R'Honi et al.* [2013] reported average NH_3 emission ratios ranging from 0.010 to 0.052. Our emission ratios are slightly larger than the values from aircraft and TES observations but agree with the lower limit from *R'Honi et al.* [2013]. Since the 2010 Russian fires included peatland burning [*Konovalov et al.*, 2011] in addition to boreal forest, the larger NH_3 emission ratios from *R'Honi et al.* [2013] are likely due to peatland burning.

The good agreement of the emission ratios of NH_3 between both sites and previous literature values assuming a 48 h lifetime suggests that the NH_3 lifetime is enhanced within a smoke plume. Bidirectional exchange of NH_3 between the atmosphere and the surface has been noted to increase NH_3 atmospheric concentrations and lifetimes [*Zhu et al.*, 2015]. However, the effects of bidirectional exchange are limited to the boundary layer and are of a different order of magnitude compared to the column enhancements due to transported biomass burning plumes. NH_3 may react rapidly with acidic gases to form ammonium particles [*Hertel et al.*, 2012], which could then be transported over large distances with lifetimes of 1–15 days [*Karlsson et al.*, 2013], therefore extending the spatial extent over which ammonia may be deposited. However, the abundance of other reactive trace gases and preexisting aerosol loads in a fire plume remains poorly known. It is possible that aerosol-gas exchange of NH_3 may extend the lifetime and long-range transport of NH_3 in a fire plume, although the magnitude of these effects is highly uncertain.

3.4. Emission Factors

Trace gas emissions from biomass burning are characterized by the emission factor. The emission factor is defined by [*Andreae and Merlet*, 2001]:

$$EF_X = EF_{CO} \cdot ER_X \cdot \left(\frac{MW_X}{MW_{CO}} \right), \quad (2)$$

where MW is the molecular weight. To convert our emission ratios to equivalent emission factors, the emission factor of CO from *Akagi et al.* [2011] was used, which is based on a compilation of studies for boreal forest fuel types. Both *Akagi et al.* [2011] and *Andreae and Merlet* [2001] report emission factors for HCN, C_2H_6, and NH_3 that can be compared to our calculated values (see Table 1). The values reported in *Andreae and Merlet* [2001] correspond to an extratropical fuel type that is a combination of boreal and temperate forests. Literature values for emission ratios and emission factors for boreal forests derived from ground-based, aircraft, and satellite platforms are also included in Table 1.

The emission factor for CO of 127 ± 45 g kg^{-1} from *Akagi et al.* [2011] was used here to convert our calculated emission ratios to emission factors. As a result, differences in emission factors between sites are due to the same differences in the emission ratios discussed in section 3.3. For HCN, our emission factor for Eureka (0.40±0.13 g kg^{-1}) is smaller than the compilation studies [*Akagi et al.*, 2011; *Andreae and Merlet*, 2001] and the aircraft-based studies [*Goode et al.*, 2000; *Simpson et al.*, 2011] but agrees within the combined uncertainties with the ground-based [*Viatte et al.*, 2015] and satellite [*Rinsland et al.*, 2007] studies. Similarly, our emission factor for C_2H_6 and those determined by ground-based [*Viatte et al.*, 2015] and satellite platforms [*Rinsland et al.*, 2007] are generally larger than that for aircraft studies [*Nance et al.*, 1993; *Goode et al.*, 2000]. For NH_3 with a lifetime of 48 h, our emission factors agree within the uncertainties with the compilation studies [*Andreae and Merlet*, 2001; *Akagi et al.*, 2011] but are larger than the aircraft-based studies of *Nance et al.* [1993] and *Goode et al.* [2000]. These differences are likely to be the result of lower emission factors of CO reported by *Nance et al.* [1993] and *Goode et al.* [2000] since the emission ratios of NH_3 were found to agree as stated in section 3.3.

4. Conclusions

The first long-term measurements of NH_3 in the Canadian Arctic have been presented here. Total columns of CO, HCN, C_2H_6, and NH_3 were measured by ground-based FTIR spectrometers at Eureka, Nunavut, and Toronto, Ontario. Emission ratios for HCN, C_2H_6, and NH_3 with respect to CO were determined for both sites.

The observed NH_3 enhancements at Eureka indicate that the 2014 Northwest Territories fires were a considerable episodic source of NH_3 to the Canadian Arctic. Simultaneous enhancements of CO, HCN, and C_2H_6 at Eureka, along with FLEXPART sensitivity runs, provided confirmation that the detected NH_3 enhancements originated from the Northwest Territories fires. Detection of simultaneous enhancements of all species at Toronto further demonstrated the long-range transport of NH_3 emissions from these fires. The consistency of the emission ratios for HCN, C_2H_6, and NH_3 with respect to CO between the two sites and literature values, particularly for NH_3 with a estimated lifetime of 48 h, provides further confidence in these observations.

Acknowledgments
This work was supported by the CAFTON project, funded by the Canadian Space Agency's FAST Program. Measurements at TAO have been supported by CFCAS, ABB Bomem, CFI, CSA, EC, NSERC, ORDCF, PREA, and the University of Toronto. Measurements at Eureka were made by CANDAC, which has been supported by the AIF/NSRIT, CFI, CFCAS, CSA, EC, Government of Canada IPY funding, NSERC, OIT, ORF, PCSP, and FQRNT. The Vrije Universiteit Amsterdam contribution was supported by the research program GO/12-36, which is financed by the Netherlands Organisation for Scientific Research. The authors gratefully acknowledge the NOAA Air Resources Laboratory for the provision of the HYSPLIT transport and dispersion model. We acknowledge the use of FIRMS data and imagery from the Land, Atmosphere Near real-time Capability for EOS system operated by the NASA/GSFC/Earth Science Data and Information System with funding provided by NASA/HQ. The authors also acknowledge the use of the FLEXPART Lagrangian dispersion model (https://www.flexpart.eu/wiki/FpDownloads) and the use of the Pflexible Python module (https://bitbucket.org/jfburkhart/pflexible) developed by John F. Burkhart, which was modified here to plot the FLEXPART sensitivities in this paper. The NCEP GFS and MODIS data used are listed in the references, and the FTIR data are available in the NDACC data repository at http://www.ndsc.ncep.noaa.gov/data/.

References

Akagi, S. K., R. J. Yokelson, C. Wiedinmyer, M. J. Alvarado, J. S. Reid, T. Karl, J. D. Crounse, and P. O. Wennberg (2011), Emission factors for open and domestic biomass burning for use in atmospheric models, *Atmos. Chem. Phys.*, *11*(9), 4039–4072, doi:10.5194/acp-11-4039-2011.

Alvarado, M. J., K. E. Cady-Pereira, Y. Xiao, D. B. Millet, and V. H. Payne (2011), Emission ratios for ammonia and formic acid and observations of Peroxy Acetyl Nitrate (PAN) and ethylene in biomass burning smoke as seen by the Tropospheric Emission Spectrometer (TES), *Atmosphere*, *2*(4), 633–654, doi:10.3390/atmos2040633.

Andreae, M. O., and P. Merlet (2001), Emission of trace gases and aerosols from biomass burning, *Global Biogeochem. Cycles*, *15*(4), 955–966, doi:10.1029/2000GB001382.

Aneja, V., B. Bunton, J. Walker, and B. Malik (2001), Measurement and analysis of atmospheric ammonia emissions from anaerobic lagoons, *Atmos. Environ.*, *35*(11), 1949–1958, doi:10.1016/S1352-2310(00)00547-1.

Batchelor, R. L., K. Strong, R. Lindenmaier, R. L. Mittermeier, H. Fast, J. R. Drummond, and P. F. Fogal (2009), A new Bruker IFS 125HR FTIR spectrometer for the Polar Environment Atmospheric Research Laboratory at Eureka, Nunavut, Canada: Measurements and comparison with the existing Bomem DA8 spectrometer, *J. Atmos. Ocean. Technol.*, *26*(7), 1328–1340.

Behera, S. N., M. Sharma, V. P. Aneja, and R. Balasubramanian (2013), Ammonia in the atmosphere: A review on emission sources, atmospheric chemistry and deposition on terrestrial bodies, *Environ. Sci. Pollut. Res.*, *20*(11), 8092–8131, doi:10.1007/s11356-013-2051-9.

Blackall, T. D., L. J. Wilson, M. R. Theobald, C. Milford, E. Nemitz, J. Bull, P. J. Bacon, K. C. Hamer, S. Wanless, and M. A. Sutton (2007), Ammonia emissions from seabird colonies, *Geophys. Res. Lett.*, *34*(10), L10801, doi:10.1029/2006GL028928.

Bobbink, R., M. Hornung, and J. G. M. Roelofs (1998), The effects of air-borne nitrogen pollutants on species diversity in natural and semi-natural european vegetation, *J. Ecol.*, *86*(5), 717–738, doi:10.1046/j.1365-2745.1998.8650717.x.

Bobbink, R., et al. (2010), Global assessment of nitrogen deposition effects on terrestrial plant diversity: A synthesis, *Ecol. Appl.*, *20*(1), 30–59, doi:10.1890/08-1140.1.

Bouwman, A., D. Lee, W. Asman, F. Dentener, K. Van Der Hoek, and J. Olivier (1997), A global high-resolution emission inventory for ammonia, *Global Biogeochem. Cycles*, *11*(4), 561–587.

Cicerone, R. J., and R. Zellner (1983), The atmospheric chemistry of hydrogen cyanide (HCN), *J. Geophys. Res.*, *88*(C15), 10,689–10,696, doi:10.1029/JC088iC15p10689.

Dammers, E., et al. (2015), Retrieval of ammonia from ground-based FTIR solar spectra, *Atmos. Chem. Phys.*, *15*(22), 12,789–12,803, doi:10.5194/acp-15-12789-2015.

Daniel, J. S., and S. Solomon (1998), On the climate forcing of carbon monoxide, *J. Geophys. Res.*, *103*(D11), 13,249–13,260, doi:10.1029/98JD00822.

Dentener, F. J., and P. J. Crutzen (1994), A three-dimensional model of the global ammonia cycle, *J. Atmos. Chem.*, *19*(4), 331–369, doi:10.1007/BF00694492.

Erisman, J. W., J. Galloway, S. Seitzinger, A. Bleeker, and K. Butterbach-Bahl (2011), Reactive nitrogen in the environment and its effect on climate change, *Curr. Opin. Environ. Sustainab.*, *3*(5), 281–290, doi:10.1016/j.cosust.2011.08.012, carbon and nitrogen cycles.

Eyring, V., et al. (2007), Multimodel projections of stratospheric ozone in the 21st century, *J. Geophys. Res.*, *112*, D16303, doi:10.1029/2006JD008332.

Giglio, L., G. R. van der Werf, J. T. Randerson, G. J. Collatz, and P. Kasibhatla (2006), Global estimation of burned area using MODIS active fire observations, *Atmos. Chem. Phys.*, *6*(4), 957–974, doi:10.5194/acp-6-957-2006.

Goode, J. G., R. J. Yokelson, D. E. Ward, R. A. Susott, R. E. Babbitt, M. A. Davies, and W. M. Hao (2000), Measurements of excess O_3, CO_2, CO, CH_4, C_2H_4, C_2H_2, HCN, NO, NH_3, HCOOH, CH_3COOH, HCHO, and CH_3OH in 1997 Alaskan biomass burning plumes by airborne Fourier transform infrared spectroscopy (AFTIR), *J. Geophys. Res.*, *105*(D17), 22,147–22,166, doi:10.1029/2000JD900287.

Hertel, O., et al. (2012), Governing processes for reactive nitrogen compounds in the European atmosphere, *Biogeosciences*, *9*(12), 4921–4954, doi:10.5194/bg-9-4921-2012.

Holloway, T., H. Levy, and P. Kasibhatla (2000), Global distribution of carbon monoxide, *J. Geophys. Res.*, *105*(D10), 12,123–12,147, doi:10.1029/1999JD901173.

Karlsson, P. E., et al. (2013), Biomass burning in Eastern Europe during spring 2006 caused high deposition of ammonium in Northern Fennoscandia, *Environ. Pollut.*, *176*, 71–79, doi:10.1016/j.envpol.2012.12.006.

Konovalov, I. B., M. Beekmann, I. N. Kuznetsova, A. Yurova, and A. M. Zvyagintsev (2011), Atmospheric impacts of the 2010 Russian wildfires: Integrating modelling and measurements of an extreme air pollution episode in the Moscow region, *Atmos. Chem. Phys.*, *11*(19), 10,031–10,056, doi:10.5194/acp-11-10031-2011.

Lefer, B. L., R. W. Talbot, and J. W. Munger (1999), Nitric acid and ammonia at a rural northeastern U.S. site, *J. Geophys. Res.*, *104*(D1), 1645–1661, doi:10.1029/1998JD100016.

Li, Q., D. J. Jacob, R. M. Yantosca, C. L. Heald, H. B. Singh, M. Koike, Y. Zhao, G. W. Sachse, and D. G. Streets (2003), A global three-dimensional model analysis of the atmospheric budgets of HCN and CH_3CN: Constraints from aircraft and ground measurements, *J. Geophys. Res.*, *108*(D21), 8827, doi:10.1029/2002JD003075.

Macias Fauria, M., and E. Johnson (2008), Climate and wildfires in the North American boreal forest, *Philos. Trans. R. Soc. B*, *363*(1501), 2315–2327, doi:10.1098/rstb.2007.2202.

Mahieu, E., R. Zander, L. Delbouille, P. Demoulin, G. Roland, and C. Servais (1997), Observed trends in total vertical column abundances of atmospheric gases from IR solar spectra recorded at the Jungfraujoch, *J. Atmos. Chem.*, *28*(1–3), 227–243, doi:10.1023/A:1005854926740.

Meier, A., G. C. Toon, C. P. Rinsland, A. Goldman, and F. Hase (2004), Spectroscopic Atlas of Atmospheric Microwindows in the Middle Infra-Red, *IRF Tech. Rep.*, vol. 048, 608 pp., Swedish Inst. of Space Phys., Kiruna, Sweden.

Nance, J. D., P. V. Hobbs, L. F. Radke, and D. E. Ward (1993), Airborne measurements of gases and particles from an Alaskan wildfire, *J. Geophys. Res.*, *98*(D8), 14,873–14,882, doi:10.1029/93JD01196.

Notholt, J., G. C. Toon, R. Lehmann, B. Sen, and J.-F. Blavier (1997), Comparison of Arctic and Antarctic trace gas column abundances from ground-based Fourier transform infrared spectrometry, *J. Geophys. Res.*, *102*(D11), 12,863–12,869, doi:10.1029/97JD00358.

Notholt, J., G. C. Toon, C. P. Rinsland, N. S. Pougatchev, N. B. Jones, B. J. Connor, R. Weller, M. Gautrois, and O. Schrems (2000), Latitudinal variations of trace gas concentrations in the free troposphere measured by solar absorption spectroscopy during a ship cruise, *J. Geophys. Res.*, *105*(D1), 1337–1349, doi:10.1029/1999JD900940.

Paton-Walsh, C., N. B. Jones, S. R. Wilson, V. Haverd, A. Meier, D. W. T. Griffith, and C. P. Rinsland (2005), Measurements of trace gas emissions from Australian forest fires and correlations with coincident measurements of aerosol optical depth, *J. Geophys. Res.*, *110*(D24), D24305, doi:10.1029/2005JD006202.

Paton-Walsh, C., N. M. Deutscher, D. W. T. Griffith, B. W. Forgan, S. R. Wilson, N. B. Jones, and D. P. Edwards (2010), Trace gas emissions from savanna fires in northern Australia, *J. Geophys. Res.*, *115*(D16), D16314, doi:10.1029/2009JD013309.

Pope, C. A. I., M. Ezzati, and D. W. Dockery (2009), Fine-particulate air pollution and life expectancy in the United States, *N. Engl. J. Med.*, *360*(4), 376–386, doi:10.1056/NEJMsa0805646.

Pougatchev, N. S., B. J. Connor, and C. P. Rinsland (1995), Infrared measurements of the ozone vertical distribution above Kitt Peak, *J. Geophys. Res.*, *100*(D8), 16,689–16,697, doi:10.1029/95JD01296.

R'Honi, Y., L. Clarisse, C. Clerbaux, D. Hurtmans, V. Duflot, S. Turquety, Y. Ngadi, and P.-F. Coheur (2013), Exceptional emissions of NH_3 and HCOOH in the 2010 Russian wildfires, *Atmos. Chem. Phys.*, *13*(8), 4171–4181, doi:10.5194/acp-13-4171-2013.

Rinsland, C. P., et al. (1998), Northern and southern hemisphere ground-based infrared spectroscopic measurements of tropospheric carbon monoxide and ethane, *J. Geophys. Res.*, *103*(D21), 28,197–28,217.

Rinsland, C. P., A. Meier, D. W. T. Griffith, and L. S. Chiou (2001), Ground-based measurements of tropospheric CO, C_2H_6, and HCN from Australia at 34°S latitude during 1997–1998, *J. Geophys. Res.*, *106*(D18), 20,913–20,924, doi:10.1029/2000JD000318.

Rinsland, C. P., N. B. Jones, B. J. Connor, S. W. Wood, A. Goldman, T. M. Stephen, F. J. Murcray, L. S. Chiou, R. Zander, and E. Mahieu (2002), Multiyear infrared solar spectroscopic measurements of HCN, CO, C_2H_6, and C_2H_2 tropospheric columns above Lauder, New Zealand (45°S latitude), *J. Geophys. Res.*, *107*(D14), 4185, doi:10.1029/2001JD001150.

Rinsland, C. P., G. Dufour, C. D. Boone, P. F. Bernath, L. Chiou, P.-F. Coheur, S. Turquety, and C. Clerbaux (2007), Satellite boreal measurements over Alaska and Canada during June–July 2004: Simultaneous measurements of upper tropospheric CO, C_2H_6, HCN, CH_3Cl, CH_4, C_2H_2, CH_3OH, HCOOH, OCS, and SF_6 mixing ratios, *Global Biogeochem. Cycles*, *21*, GB3008, doi:10.1029/2006GB002795.

Rodgers, C. (2000), *Inverse Methods for Atmospheric Sounding: Theory and Practice, Series on Atmospheric*, World Scientific, Aceanic and Planetary Physics.

Rolph, G. D. (2016), *Real-Time Environmental Applications and Display System (READY)*, NOAA Air Res. Lab., College Park, Md.

Rothman, L. S., L. Gordon, A. Barbe, D. Benner, P. Bernath, M. Birk, V. Boudon, L. R. Brown, A. Campargue, and J. Champion (2009), The HITRAN 2008 molecular spectroscopic database, *J. Quant. Spectros. Radiat. Transfer*, *110*(9), 533–572.

Saha, S., et al. (2011), *NCEP Climate Forecast System Version 2 (CFSv2) 6-hourly Products*, Res. Data Archive at the Natl. Cent. for Atmos. Res., Comput. and Info. Syst. Lab., Boulder, Colo., doi:10.5065/D61C1TXF.

Simpson, I. J., et al. (2011), Boreal forest fire emissions in fresh Canadian smoke plumes: C_1-C_{10} volatile organic compounds (VOCs), CO_2, CO, NO_2, NO, HCN and CH_3CN, *Atmos. Chem. Phys.*, *11*(13), 6445–6463, doi:10.5194/acp-11-6445-2011.

Singh, H. B., and P. Zimmerman (1992), Atmospheric distribution and sources of nonmethane hydrocarbons, in *Gasesous Pollutants: Characterization and Cycling*, p. 235, Jon Wiley, New York.

Stein, A. F., R. R. Draxler, G. D. Rolph, B. J. B. Stunder, M. D. Cohen, and F. Ngan (2015), NOAA's HYSPLIT atmospheric transport and dispersion modeling system, *Bull. Am. Meteorol. Soc.*, *96*, 2059–2077, doi:10.1175/BAMS-D-14-00110.1.

Stohl, A., C. Forster, A. Frank, P. Seibert, and G. Wotawa (2005), Technical note: The Lagrangian particle dispersion model FLEXPART version 6.2, *Atmos. Chem. Phys.*, *5*, 2461–2474, doi:10.5194/acp-5-2461-2005.

Tereszchuk, K. A., G. González Abad, C. Clerbaux, J. Hadji-Lazaro, D. Hurtmans, P.-F. Coheur, and P. F. Bernath (2013), ACE-FTS observations of pyrogenic trace species in boreal biomass burning plumes during BORTAS, *Atmos. Chem. Phys.*, *13*(9), 4529–4541, doi:10.5194/acp-13-4529-2013.

Theobald, M. R., P. D. Crittenden, A. P. Hunt, Y. S. Tang, U. Dragosits, and M. A. Sutton (2006), Ammonia emissions from a Cape fur seal colony, Cape Cross, Namibia, *Geophys. Res. Lett.*, *33*, L03812, doi:10.1029/2005GL024384.

Toon, G. C., et al. (1999), Comparison of MkIV balloon and ER-2 aircraft measurements of atmospheric trace gases, *J. Geophys. Res.*, *104*(D21), 26,779–26,790, doi:10.1029/1999JD900379.

Viatte, C., K. Strong, C. Paton-Walsh, J. Mendonca, N. O'Neill, and J. Drummond (2013), Measurements of CO, HCN, and C_2H_6 total columns in smoke plumes transported from the 2010 Russian boreal forest fires to the Canadian high Arctic, *Atmos. Ocean*, *51*(5), 522–531.

Viatte, C., K. Strong, K. A. Walker, and J. R. Drummond (2014), Five years of CO, HCN, C_2H_6, C_2H_2, CH_3OH, HCOOH and H_2CO total columns measured in the Canadian high Arctic, *Atmos. Meas. Tech.*, *7*(6), 1547–1570, doi:10.5194/amt-7-1547-2014.

Viatte, C., K. Strong, J. Hannigan, E. Nussbaumer, L. K. Emmons, S. Conway, C. Paton-Walsh, J. Hartley, J. Benmergui, and J. Lin (2015), Identifying fire plumes in the Arctic with tropospheric FTIR measurements and transport models, *Atmos. Chem. Phys.*, *15*(5), 2227–2246, doi:10.5194/acp-15-2227-2015.

Vigouroux, C., et al. (2012), FTIR time-series of biomass burning products (HCN, C_2H_6, C_2H_2, CH_3OH, and HCOOH) at Reunion Island (21°; S, 55°E) and comparisons with model data, *Atmos. Chem. Phys.*, *12*(21), 10,367–10,385, doi:10.5194/acp-12-10367-2012.

Wentworth, G. R., et al. (2016), Ammonia in the summertime arctic marine boundary layer: Sources, sinks, and implications, *Atmos. Chem. Phys.*, *16*(4), 1937–1953, doi:10.5194/acp-16-1937-2016.

Whaley, C. H., et al. (2015), Toronto area ozone: Long-term measurements and modeled sources of poor air quality events, *J. Geophys. Res. Atmos.*, *120*, 11,368–11,390, doi:10.1002/2014JD022984.

Whitburn, S., M. V. Damme, J. Kaiser, G. van der Werf, S. Turquety, D. Hurtmans, L. Clarisse, C. Clerbaux, and P.-F. Coheur (2015), Ammonia emissions in tropical biomass burning regions: Comparison between satellite-derived emissions and bottom-up fire inventories, *Atmos. Environ.*, *121*, 42–54, doi:10.1016/j.atmosenv.2015.03.015.

Wiacek, A., J. R. Taylor, K. Strong, R. Saari, N. B. Jones, and D. W. T. Griffith (2007), Ground-based solar absorption FTIR spectroscopy: Characterization of retrievals and first results from a novel optical design instrument at a new NDACC complementary station, *J. Atmos. Ocean. Technol.*, *24*(3), 432–448.

Xiao, Y., J. A. Logan, D. J. Jacob, R. C. Hudman, R. Yantosca, and D. R. Blake (2008), Global budget of ethane and regional constraints on U.S. sources, *J. Geophys. Res.*, *113*, D21306, doi:10.1029/2007JD009415.

York, D., N. M. Evensen, M. L. Martínez, and J. De Basabe Delgado (2004), Unified equations for the slope, intercept, and standard errors of the best straight line, *Am. J. Phys.*, *72*(3), 367–375, doi:10.1119/1.1632486.

Zhao, Y., et al. (2002), Spectroscopic measurements of tropospheric CO, C_2H_6, C_2H_2, and HCN in northern Japan, *J. Geophys. Res.*, *107*(D18), 4343–4359, doi:10.1029/2001JD000748.

Zhu, L., D. Henze, J. Bash, G.-R. Jeong, K. Cady-Pereira, M. Shephard, M. Luo, F. Paulot, and S. Capps (2015), Global evaluation of ammonia bidirectional exchange and livestock diurnal variation schemes, *Atmos. Chem. Phys.*, *15*(22), 12,823–12,843, doi:10.5194/acp-15-12823-2015.